Available online at www.sciencedirect.com
SCIENCE DIRECT®
C. R. Mecanique 333 (2005) 660–665
COMPTES RENDUS MECANIQUE
http://france.elsevier.com/direct/CRAS2B/

Computational AeroAcoustics: from acoustic sources modeling to farfield radiated noise prediction

An acoustic analogy applied to the laminar upstream flow over an open 2D cavity

Jonas Ask [a,*], Lars Davidson [b]

[a] *Volvo Car Corporation, Fluid Dynamic Center, 405 31 Göteborg, Sweden*
[b] *Division of Thermo and Fluid Dynamics, Chalmers, University of Technology, 412 96 Göteborg, Sweden*

Available online 9 September 2005

Abstract

In this work a modified version of the Lighthill–Curle's analogy is applied to study the near field acoustics of an upstream laminar flow past an open cavity. Three incompressible cases have been computed and are compared against the corresponding compressible results. The three incompressible cases are carried out with different time-step sizes, distances from the cavity trailing edge to the outlet and spatial resolution in the streamwise direction. The aim of the work is to study the differences in compressible and incompressible sources in Lighthill–Curle's equation and their influence on the sound radiated. ***To cite this article: J. Ask, L. Davidson, C. R. Mecanique 333 (2005).***

Résumé

Une analogie acoustique appliquée aux écoulements dans une cavité ouverte de deux dimensions. Dans cette étude une version modifiée de l'analogie de Lighthill–Curle est utilisée pour l'étude de l'acoustique en amont d'un écoulement laminaire passant une cavité. Trois cas incompressibles sont réalisés et comparés avec leurs homologues compressibles. Les trois cas incompressibles comprennent différents pas temporels, distances séparant le bord amount du bord aval et différentes résolutions spatiales dans la direction de l'écoulement. Le but de l'étude est l'analyse des différences entre les sources compressibles et incompressibles dans l'équation de Lighthill–Curle et leur influence sur le son propagé. ***Pour citer cet article : J. Ask, L. Davidson, C. R. Mecanique 333 (2005).***

Keywords: Acoustics; Curle; Cavity; Incompressible CFD

Mots-clés : Acoustique ; Curle ; Cavité ; Incompressible CFD

* Corresponding author.
E-mail addresses: jask5@volvocars.com (J. Ask), lada@tfd.chalmers.se (L. Davidson).

1631-0721/$ – see front matter
doi:10.1016/j.crme.2005.07.005

1. Introduction

The aim of this work is to study the effects of Lighthill–Curle's analogy applied to incompressible CFD (Computational Fluid Dynamics). The basic assumption is that the density fluctuations can be neglected for low Mach number flows. The sound generation and propagation can then be estimated by the sources evaluated from an incompressible flow field.

The method is based on a two step procedure for evaluating the sound pressure level at an observer point. The first step is based on extracting information from a transient incompressible CFD solution. In this case the two dipole source terms include the wall pressure and the time derivative of the wall pressure. These terms have previously been identified as the two dominating terms [1] and are the terms treated in this work.

Open cavities have been the subject of both experimental [2,3] and numerical studies [4,5] in recent years. These studies focus at the mode shift of the flow when altering the L/D ratio and the upstream boundary layer thickness, where D is cavity depth and L is the cavity length. Additional numerical studies conducted by [6,1] use acoustic analogies to compute the radiated sound and compare the results against compressible direct numerical simulations. In this work the compressible direct numerical simulation serves as a reference for the acoustic sources computed by an incompressible direct numerical simulation. When this assumption is made, one is forced to use an acoustic analogy due to the fact that sound waves are not present in the computational domain.

2. The flow field

The investigated case is the flow over an open cavity with an upstream laminar profile at a corresponding Mach number of 0.15. The Reynolds number is $Re_D = 1500$, based on the cavity depth and the freestream velocity. A more thorough examination of the flow field under these circumstances were conducted in [1]. The investigated parameters for the different cases are given in Table 1. All cases except Case 1 have uniformly distributed mesh in the cavity with 80 cells in the x_2 direction and 60 cells per unit length in the x_1 direction. The mesh over the inlet wall has 60 cells (constant Δx) per unit length in the x_1 direction. Over the outlet wall the mesh is stretched less than 0.6 percent for Case 2 and Case 3. Case 1 is roughly twice as coarse as the other cases. The case 'Ref' is the compressible reference case and more information regarding methodology, boundary conditions and discretization schemes can be found in [1].

For the incompressible approach more information can be found in [7] regarding cavity drag and the Strouhal number. The solver used for this purpose is the incompressible FVM (Finite Volume Method) code CALC-BFC [8] using a second order spatial Van Leer scheme for the convective fluxes in combination with a second order Crank–Nickolson time marching scheme. A spatial second order central scheme have also been tested but no major difference in source intensities or radiated sound were found for the coarser case. The pressure is coupled to the velocity field through the SIMPLEC pressure correction algorithm and the computational mesh is based on a single block arrangement with blockage outside the fluid domain.

Table 1
The parameters investigated

Case	Δt	Trailing edge to outlet	Nodes in x_1-direction
Ref	0.001	$15D$	1270
Case 1	0.001	$10D$	460
Case 2	0.005	$15D$	900
Case 3	0.001	$15D$	900

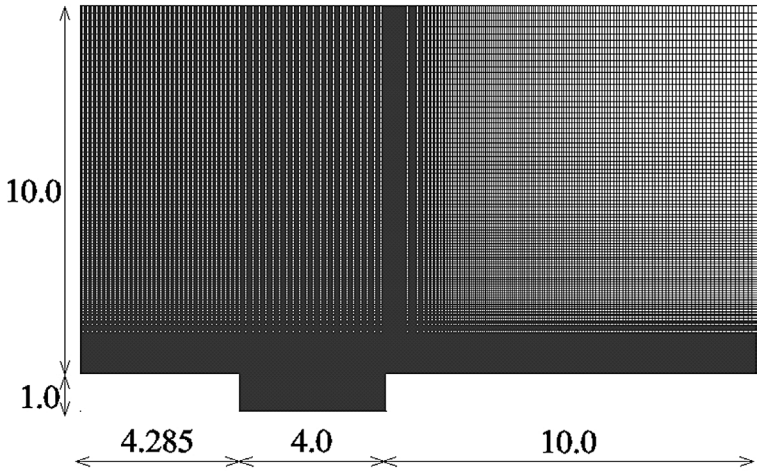

Fig. 1. Geometrical dimensions for Case 1.

Fig. 1. Dimensions géométriques pour le Cas 1.

The following boundary conditions are used, symmetry at the far field boundary and no slip condition at the walls. Predefined velocity profiles for U and V at the inlet, extracted from an averaged compressible inflow profile 4.285D upstream the cavity leading edge. At the outlet a convective outlet boundary condition is used

$$\frac{\partial u_i}{\partial t} + U_c \frac{\partial u_i}{\partial x} = 0 \tag{1}$$

where U_c is the bulk velocity. This boundary condition is normally used for incompressible flow fields where vorticity might be present at the outflow and has successfully been used by [9] and [10]. In a discretized form Eq. (1) can be written as

$$u_{ni}^{t} = (1 - C)u_{ni}^{t-1} + Cu_{ni-1}^{t-1} \tag{2}$$

where C is the Courant number defined as, $C = U_c \Delta t / \Delta x$.

3. The acoustic field

A modified version of Lighthill–Curle's equation is used in this work with temporal derivatives inside the integral instead of keeping the spatial derivatives outside the integral, as Curle's [11] original formulation states. The derivation can be found in [12] as the time integral solution of a retarded time problem keeping both near and farfield terms.

$$\begin{aligned} p(\mathbf{x}, t) - p_\infty = {} & \frac{1}{4\pi} \int_V \left[\frac{l_i l_j}{a_\infty^2 r} \ddot{T}_{ij} + \frac{3l_i l_j - \delta_{ij}}{a_\infty r^2} \dot{T}_{ij} + \frac{3l_i l_j - \delta_{ij}}{r^3} T_{ij} \right] \mathrm{d}V(\mathbf{y}) \\ & + \frac{1}{4\pi} \int_S l_i n_j \left[\frac{\dot{p}\delta_{ij} - \dot{\tau}_{ij}}{a_\infty r} + \frac{p\delta_{ij} - \tau_{ij}}{r^2} \right] \mathrm{d}S(\mathbf{y}) \end{aligned} \tag{3}$$

Eq. (3) is valid for three dimensions while the flow field is computed in two dimensions. This is solved by expanding the solution in the spanwise direction. A sensitivity study of this expansion was conducted in [1]. In the following, source term 1 and 2 will refer to the wall pressure and the time derivative of the wall pressure, respectively.

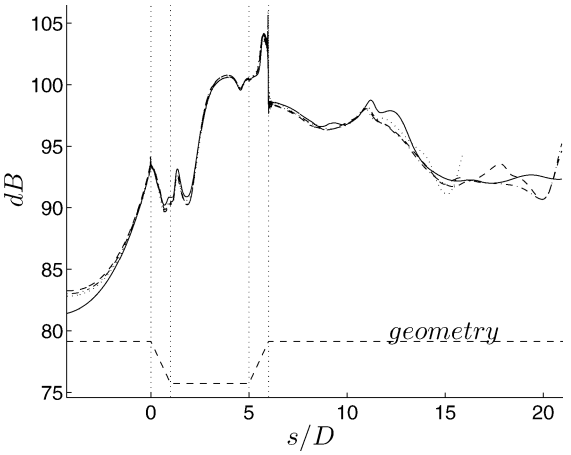

Fig. 2. Wall source intensity for term 1, (-) Ref, (..) Case 1, (- -) Case 2, (.-) Case 3.

Fig. 2. Intensité des sources de paroi pour le terme 1, (-) Ref, (..) Cas 1, (- -) Cas 2, (.-) Cas 3.

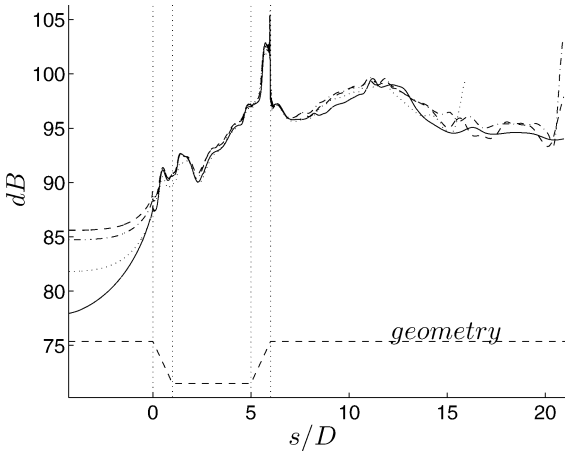

Fig. 3. Wall source intensity for term 2, (-) Ref, (..) Case 1, (- -) Case 2, (.-) Case 3.

Fig. 3. Intensité des sources de paroi pour le terme 2, (-) Ref, (..) Cas 1, (- -) Cas 2, (.-) Cas 3.

In Figs. 2 and 3 the wall source intensity for the reference case and the three incompressible cases are presented. The source intensity is defined as:

$$S_l = 20\log_{10}\left[\frac{\phi_{l,\mathrm{rms}}}{\phi_{l,\mathrm{ref}}}\right] \tag{4}$$

where, $\phi_{l,\mathrm{ref}} = \sqrt{\rho_\infty a_\infty \times 10^{-12}}$ and the subscript l represents the source term index. In the two figures the geometry is folded out to visualize the results over the two vertical walls and gives information of the source magnitude of the two source terms. Over the cavity walls all cases shows good agreement, but when approaching the inlet and outlet some discrepancies can be found especially for source term 2. Regarding the inlet, the discrepancy can be explained by the applied boundary condition and its close proximity to the cavity leading edge. Close to the outlet, peaks in the wall source intensity can be seen for all incompressible cases. These systematic discrepancies show an over prediction of the wall pressure fluctuations possibly due to the applied outlet boundary condition.

The radiated sound for 9 observers at $-2.0D < x_1 < 6.0D$, $x_2 = 7.18D$, is presented in Figs. 4–7. The figures show how the sound directivity of the radiated sound changes when increasing the surface integration area.

In Fig. 4 the surface integration extends over the three cavity walls showing good agreement for all cases and supports the findings in Figs. 2 and 3. When extending the surface integration over the inlet wall a 1 dB offset between the incompressible and the compressible case can be found, Fig. 5. As pointed out previously this offset can be explained by the inlet boundary condition. The offset is however rather small and the directivity is kept. In Fig. 6 a section of the outflow wall is included in the surface integration. The compressible case levels out for the most downstream positioned observer while the incompressible cases shows a negative slope. However the magnitude for both terms are well predicted for this additional wall slice according to Figs. 2 and 3. The levels over this surface slice are much higher than over the inlet wall and small discrepancies in source strengths can cause the discrepancy when integrating in the spanwise direction. The last figure in this series is Fig. 7 where the surface integration extends over the whole Case 2 wall domain. A maximum discrepancy of 7 dB between Case 4 and the Reference case can be found over the trailing edge. The radiated sound field is however significantly different for the Reference case compared to the incompressible cases. These findings indicate that either the sources predicted from the incompressible cases have a different phase compared to the compressible case or that the existing discrepancy in the wall source intensity causes the different shape in the radiated sound field.

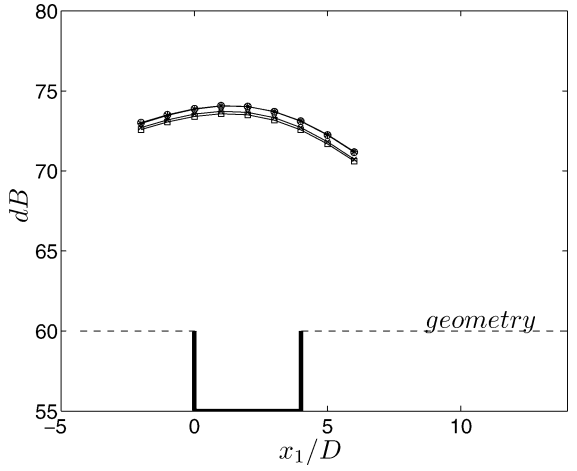

Fig. 4. SPL for observers, $-2.0D < x_1 < 6.0D$, $x_2 = 7.18D$, □ Ref, × Case 1, ⋆ Case 2, ○ Case 3.

Fig. 4. Niveau de pression sonore pour l'observateur, □ Ref, × Cas 1, ⋆ Cas 2, ○ Cas 3.

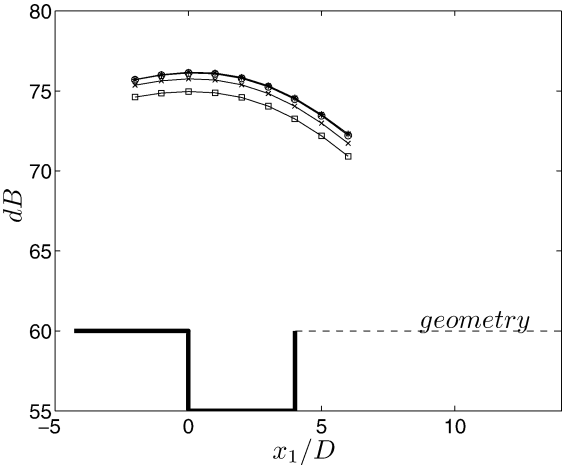

Fig. 5. SPL for observers, $-2.0D < x_1 < 6.0D$, $x_2 = 7.18D$, □ Ref, × Case 1, ⋆ Case 2, ○ Case 3.

Fig. 5. Niveau de pression sonore pour l'observateur, □ Ref, × Cas 1, ⋆ Cas 2, ○ Cas 3.

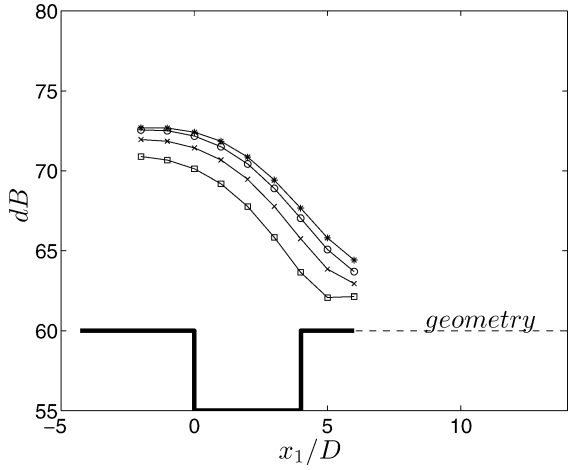

Fig. 6. SPL for observers, $-2.0D < x_1 < 6.0D$, $x_2 = 7.18D$, □ Ref, × Case 1, ⋆ Case 2, ○ Case 3.

Fig. 6. Niveau de pression sonore pour l'observateur, □ Ref, × Cas 1, ⋆ Cas 2, ○ Cas 3.

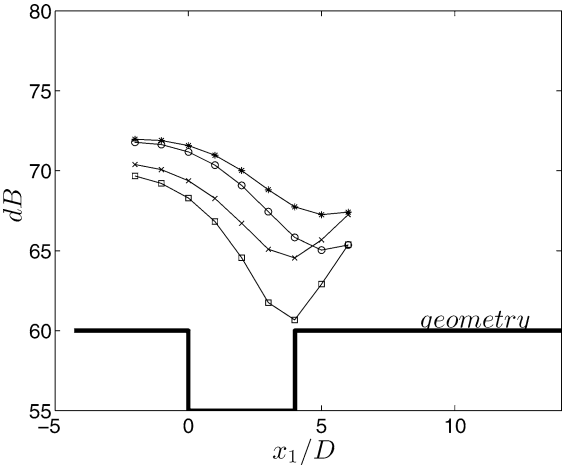

Fig. 7. SPL for observers, $-2.0D < x_1 < 6.0D$, $x_2 = 7.18D$, □ Ref, × Case 1, ⋆ Case 2, ○ Case 3.

Fig. 7. Niveau de pression sonore pour l'observateur, □ Ref, × Cas 1, ⋆ Cas 2, ○ Cas 3.

The last results presented in this work are an attempt to study the background pressure when vortices are convected out of the domain, Figs. 8 and 9. This attempt was raised due to the findings in the wall source intensities close to the outlet for the incompressible cases. When vortices convect over the outlet a pressure drop occurs locally for the outlet monitor point. As can be seen this causes small disturbances in the whole domain but does not explain the high levels at the outlet, at least for the pressure term. The question whether the increased levels in the wall source strengths is a consequence of the applied outlet boundary condition is still unanswered.

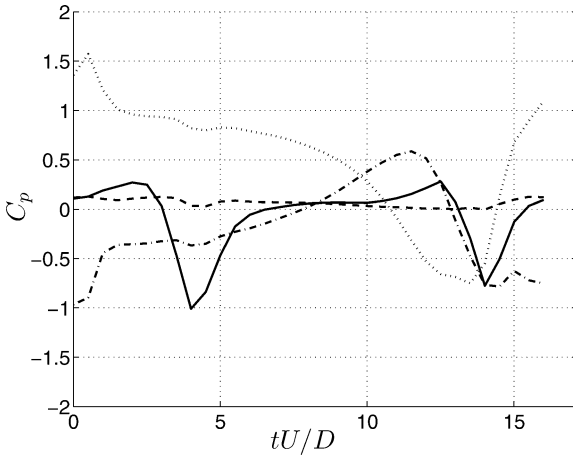

Fig. 8. C_p for four different positions for Case 2, (-) $x_1 = 19$, $x_2 = 0.5$, (..) $x_1 = 4$, $x_2 = -0.5$, (--) $x_1 = -4.1$, $x_2 = 9.9$, (.-) $x_1 = 4.1$, $x_2 = 0$.

Fig. 8. C_p, à différentes positions pour le Cas 2.

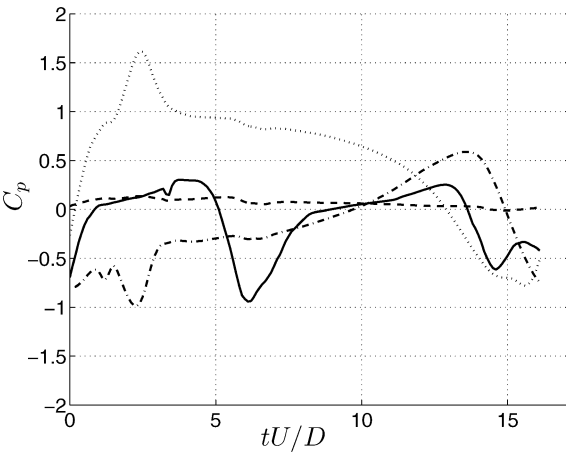

Fig. 9. C_p for four different positions for Case 3, (-) $x_1 = 19$, $x_2 = 0.5$, (..) $x_1 = 4$, $x_2 = -0.5$, (--) $x_1 = -4.1$, $x_2 = 9.9$, (.-) $x_1 = 4.1$, $x_2 = 0$.

Fig. 9. C_p, à différentes positions pour le Cas 4.

4. Conclusion

Results from three incompressible cases are presented and compared against a compressible reference case. It is shown that the incompressible approach gives acceptable results when estimating wall source intensities. When considering the radiated sound additional studies of what causes the discrepancies over the outlet wall and the outlet have to be investigated. The outlet boundary condition introduces high intensities close to the outlet and should be improved in future studies. The sound directivity is porly predicted when including the outlet wall in the surface integration even if the wall source intensities are generally well predicted. This can be caused if a phase mismatch between compressible and incompressible sources exists.

Acknowledgements

This work was supported by Volvo Cars Corporation and the Swedish Agency for Innovation Systems (VINNOVA).

References

[1] J. Larsson, Computational Aero Acoustics for vehicle applications, Chalmers University of Technology, 2002.
[2] M. Gharib, A. Roshko, The effect of flow oscillations on cavity drag, J. Fluid Mech. 177 (1987) 501–530.
[3] M. Gharib, Response of the cavity shear layer oscillations to external forcing, AIAA J. 25 (1987) 43–47.
[4] T. Colonius, A.J. Basu, C.W. Rowley, Computation of sound generation and flow/acoustic instabilities in the flow past an open cavity, in: 3rd ASME/JSME Joint Fluids Engineering Conference, 1999, FEDSM99-7228.
[5] C.W. Rowley, T. Colonius, A.J. Basu, On self-sustained oscillations in two-dimensional compressible flow over rectangular cavities, J. Fluid Mech. 455 (2002) 315–346.
[6] X. Gloerfelt, C. Bailly, D. Juvé, Application de méthodes intégrales au calcul du bruit de cavité, C. R. Mecanique 330 (1) (2002) 13–20.
[7] J. Ask et al., An acoustic analogy applied to incompressible flow field, in: EUROMECH Colloquium, no 449, 2003.
[8] L. Davidsson, B. Farhanieh, CALC-BFC, A finite-volume code employing collocated variable arrangement and cartesian velocity components for computation of fluid flow and heat transfer in complex three-dimensional geometries, Chalmers University of Technology, Department of Thermo and Fluid Dynamics, 1995.
[9] S. Krajnovic, Large-Eddy Simulations for computing the flow around vehicles, Chalmers University of Technology, 2002.
[10] S. Dahlström, Large Eddy Simulation of the flow around a high-lift airfoil, Chalmers University of Technology, 2003.
[11] N. Curle, The influence of solid boundaries upon aerodynamic sound, Proc. Roy. Soc. London Ser. A 231 (1955) 505–514.
[12] K.S. Brentner, F. Farassat, Modeling aerodynamically generated sound of helicopter rotors, Prog. Aerospace Sci. 39 (2003) 83–120.